Journal of Molecular Structure 1353 (2026) 144633

Contents lists available at ScienceDirect

Journal of Molecular Structure

journal homepage: www.elsevier.com/locate/molstr

Structural, morphological, wettability, optical and electrical properties of Au-doped Co_3O_4

Warda Darenfad [a,*], Younes Nezzari [a], Noubeil Guermat [b,c], Kamel Mirouh [a], Nadir Bouarissa [d,*], Amor Azizi [e]

[a] Thin Films and Interfaces Laboratory (LCMI), University of Constantine 1, 25000 Constantine, Algeria
[b] Department of Electronics, Faculty of Technology, University of M'sila, University Pole, Road Bordj Bou Arreridj, 28000 M'sila, Algeria
[c] Laboratory of Electronic Materials Studies for Medical Applications (LEMSMA), University of Constantine 1, 25000 Constantine, Algeria
[d] Laboratory of Materials Physics and Its Applications, University of M'sila, 28000 M'sila, Algeria
[e] Laboratoire de Chimie, Ingénierie, Moléculaire et Nanostructures (LCIMN), Université Ferhat Abbas - Sétif 1, 19000, Sétif, Algérie

ARTICLE INFO

Keywords:
Thin films
Au-doped Co_3O_4
Spray pyrolysis
Wettability
Heterojunction

ABSTRACT

Co_3O_4 and Au-doped Co_3O_4 thin films with various Au contents (x = 1, 1.5, and 2 wt%) were successfully synthesized by spray pyrolysis method at 400 °C. X-ray diffraction confirmed the preservation of the cubic spinel Co_3O_4 structure up to 1 wt% Au, while a secondary CoO phase appeared at higher doping levels. The crystallite size increased from 6.34 nm (pure Co_3O_4) to 9.19 nm (1 wt% Au), indicating improved crystallinity. FTIR spectroscopy further confirmed the spinel vibrational modes and the presence of the CoO secondary phase. AFM revealed that the surface roughness increased with 1 wt% Au, then decreased with higher Au concentrations, in agreement with the contact angle (CA) results. The 1 wt% Au-doped film exhibited hydrophobic behavior (CA > 90°), while the others remained hydrophilic. Optical analysis showed a non-linear variation in transmittance and a redshift in the band gap (Eg_1 = 1.42 eV, Eg_2 = 2.07 eV for 2 wt% Au), attributed to impurity level formation. The lowest resistivity (6.9×10^{-1} Ω.cm) was obtained for the 1 wt% Au sample. Furthermore, the 1 wt% Au–Co_3O_4/ZnO/FTO/Glass heterojunction displayed rectifying I–V characteristics with an ideality factor of 1.65, confirming its diode-like behavior. These findings highlight the promising potential of Au-doped Co_3O4 thin films for optoelectronic and photovoltaic device applications.

1. Introduction

Cobalt oxide (Co_3O_4) has emerged as a highly promising material for thin-film optoelectronic applications due to its strong optical absorption, excellent chemical stability, and environmentally friendly characteristics. As a p-type semiconductor with a direct bandgap in the range of ~1.6–2.2 eV, Co_3O_4 has attracted significant attention as an absorber layer in thin-film solar cells [1]. However, its relatively moderate electrical conductivity and limited charge carrier mobility present critical challenges that can restrict device performance. Recent research has therefore focused on various doping strategies to fine-tune the structural, electrical, and optical properties of Co_3O_4 films, aiming to enhance their functionality for photovoltaic applications. Prior investigations have demonstrated the beneficial effects of incorporating dopants such as Ni [2], Mn [3], Fe [4], Mo [5], Cd [6], Sn [7], and Nd [8] which have been shown to directly influence the optical and/or electrical conductivity of Co_3O_4. For instance, Marnadu et al. [5] reported that the optical band gap of Mo-doped Co_3O_4 thin films exhibited slight variations with dopant concentration, with values of 2.67, 2.78, 2.62, and 2.65 eV corresponding to 0, 2, 4, and 6 wt. % Mo, respectively. Similarly, Shkir et al. [8] fabricated pure Co_3O_4 and Nd-doped Co_3O_4 thin films with Nd concentrations of 1, 3, and 5 wt. %. Their findings revealed that Nd incorporation enhanced transmission in the visible region, with the films displaying two distinct band gaps in the ranges of 2.03–2.15 eV and 1.49–1.55 eV. Furthermore, Nezzari et al. [2] observed a progressive reduction in optical transmission with increasing Ni content (0, 2, 4, and 6 %), accompanied by direct band gaps (Eg_1 and Eg_2) decreasing from 1.41 to 1.30 eV and from 2.09 to 1.99 eV, respectively. Notably, the 2 % Ni-doped Co_3O_4 film exhibited the lowest electrical resistivity, measured at 0.178 Ω·cm. In this study, we focus on exploring the effect of gold (Au) doping on Co_3O_4 thin films, prepared via the spray pyrolysis technique and deposited onto ordinary glass

* Corresponding authors.
E-mail addresses: daranfed.warda@umc.edu.dz (W. Darenfad), n_bouarissa@yahoo.fr (N. Bouarissa).

https://doi.org/10.1016/j.molstruc.2025.144633
Received 17 August 2025; Received in revised form 23 October 2025; Accepted 1 November 2025
Available online 3 November 2025

substrates. Specifically, we examine the impact of varying Au doping concentrations (0, 1, 1.5, and 2 wt %) on the crystallite size, charge carrier mobility, and overall material performance. Gold was selected as a dopant due to several anticipated advantages: (i) as Co_3O_4 is a p-type semiconductor with moderate conductivity, the introduction of Au nanoparticles or Au^{+3} ions is expected to enhance electrical conductivity by creating additional conduction pathways or reducing the film resistivity, thereby improving charge transport; (ii) gold nanoparticles exhibit localized surface plasmon resonance (LSPR), an optical phenomenon that enhances light trapping and absorption within the active material, particularly in the visible range, leading to improved electron-hole pair generation and increased photocurrent as demonstrated, for example, by Wang et al. [9], who showed that integrating Au@Pt@Au nanoparticles into perovskite solar cells increased the power conversion efficiency from 12.4 % to 13.4 % due to enhanced plasmonic light absorption; (iii) gold can act as an electron sink at the Co_3O_4 interface, reducing charge carrier recombination and facilitating the separation of photo-generated electrons and holes, thereby increasing the quantum efficiency of the device; (iv) the incorporation of Au can stabilize the chemical and structural properties of Co_3O_4, reducing surface defects and protecting the material from excessive oxidation or UV-induced degradation; and (v) in heterojunction solar cell configurations, gold can serve as an interfacial layer or ohmic contact, enhancing charge injection and collection at the electrodes. Overall, the integration of gold into Co_3O_4 absorber layers offers multiple synergistic benefits, including enhanced light absorption, improved catalytic activity (e.g., for the oxygen evolution reaction, OER), optimized electronic interfaces, and superior charge separation, all of which contribute to advancing the photovoltaic performance of thin-film solar cells. To date, significant advancements have been made in the controlled synthesis of Co_3O_4 thin films, with extensive research dedicated to optimizing both pristine and doped variants through a variety of deposition techniques. Beyond conventional chemical bath deposition, methods such as sputtering, spray pyrolysis, pulsed laser deposition, chemical vapor deposition, sol-gel processing, dip coating, and hydrothermal synthesis have been successfully employed to tailor the structural, optical, and electrical properties of Co_3O_4 films. Among these, spray pyrolysis has emerged as a particularly promising technique, offering notable advantages including operational simplicity, precise control over deposition parameters, cost-effectiveness, and the ability to achieve uniform coatings over large substrate areas making it highly suitable for scalable thin-film fabrication [10–13]. Surface wettability is a key factor influencing the performance of thin films in photovoltaic applications. Based on their water contact angle (CA), surfaces are generally categorized as hydrophilic (CA $< 90°$, [14]) or hydrophobic (CA $> 90°$, [11]). This distinction is particularly relevant for solar cells, as hydrophobic films can enhance device durability and efficiency by reducing water adhesion and shielding the active layers from moisture-related degradation [11]. Studies on p-type metal oxides have highlighted the benefits of hydrophobicity in this context [10,11,14]. For example, Nezzari et al. [2] studied Co_3O_4 thin films, both undoped and nickel-doped (2, 4, and 6 %), prepared via spray pyrolysis. They found that the film doped with 6 % Ni exhibited hydrophobicity (CA = 99°), low transmittance ($T = 20.88$ %), and dual optical band gaps ($Eg_1 = 1.3$ eV and $Eg_2 = 1.99$ eV). Nezzari et al. [10] examined the effect of different cobalt precursors (nitrate, chloride, and acetate) on Co_3O_4 films elaborated by the same method. All films showed hydrophobic behavior, but the film derived from cobalt nitrate (CA = 93°) was particularly notable for its very high absorbance ($T = 0.96$ %), a low band gap (1.32 eV), and low electrical resistivity (2.905×10^{-1} Ω.cm). Similarly, Darenfad et al. [15] demonstrated that CuO films doped with 6 % Co, in comparison to lower concentrations of 2 % and 4 %, exhibited hydrophobic behavior (CA = 97°), along with enhanced optical and electrical properties. Darenfad et al. [14] investigated the effect of deposition time on CuO films (ranging from 5 to 20 min). The film deposited for 20 min, with a contact angle of 105°, showed the lowest transmittance (6.48 %), low resistivity (3.77 Ω.cm), and a high carrier density (1.269×10^{16} cm^{-3}).

This study aims to elaborate hydrophobic Co_3O_4 thin films as absorber layers for photovoltaic applications. It investigates the impact of Au-doping at 1, 1.5, and 2 wt % on the structural, morphological, wettability, optical, and electrical properties of Co_3O_4 films deposited on glass substrates via spray pyrolysis. The goal is to deepen the understanding of how Au influences these key properties. To our knowledge, this is the first study to examine the wettability of Au:Co_3O_4 thin films produced by spray pyrolysis, underscoring the originality of this research.

2. Experimental procedure

2.1. Solution preparation

Au-doped Co_3O_4 thin films were synthesized using the spray pyrolysis technique (Fig. 1). Analytical grade cobalt nitrate hexahydrate ($Co(NO_3)_2{\cdot}6H_2O$) and gold (III) chloride solution ($HAuCl_4$) served as the cobalt and gold precursors, respectively, while deionized distilled water was used as the solvent. To prepare the precursor solutions, 0.291 g of cobalt nitrate was dissolved in 20 mL of distilled water, with gold doping concentrations of 1, 1.5, and 2 wt % incorporated at room temperature. The resulting mixtures were magnetically stirred for 30 min to ensure homogeneity. Prior to deposition, commercial glass substrates were thoroughly cleaned using acetone and distilled water in an ultrasonic bath for 30 min, followed by drying in hot air to enhance film-substrate adhesion. The possible chemical reaction during spray pyrolysis deposition is as follows:

$$(1-x)Co(NO_3)_2{\cdot}6H_2O + HAuCl_4 + H_2O \rightarrow Co_{3-x}Au_xO_4 + NO_x + Cl^- + H^+ + O_2 + H_2O$$

2.2. Preparation of undoped and Au-doped Co_3O_4 thin films

The prepared solutions were then filtered and sprayed through a fine nozzle onto preheated glass substrates maintained at 400 °C for 6 min throughout the spraying process.The nozzle-to-substrate distance was set at 17 cm, which represents an optimal balance between droplet evaporation and their deposition on the substrate. This setup enables the formation of dense and uniform films with good adhesion and uniform precursor decomposition, while also ensuring homogeneous dopant incorporation within the Co_3O_4 matrix. Compressed air at a pressure of 1 bar was used as the carrier gas. After deposition, the films were allowed to cool naturally to room temperature. The as-deposited Au:Co_3O_4 thin films were uniform in appearance, exhibiting a characteristic dark brown color.

2.3. Characterizations

Following deposition, the samples underwent comprehensive characterization to assess the properties of the thin films. Film thickness (t) was measured using a DECTAK3 profilometer. Structural analysis was carried out with a Philips X'Pert diffractometer equipped with Cu Kα radiation ($\lambda = 0.15418$ nm), providing insights into the crystalline structure of the deposited layers. Fourier-transform infrared (FTIR) spectra were recorded in the range of 400–3500 cm^{-1} using a Shimadzu FTIR spectrometer. Surface morphology was examined using a Nanosurf Flex-Axiom C3000 atomic force microscope (AFM) operating in static (contact) mode at room temperature under ambient conditions. In this mode, the AFM tip scans the surface point by point and line by line, with its movements in the x, y, and z directions detected by laser beam deflection. These deflections are recorded and processed by an optical sensor to generate a high-resolution three-dimensional image of the surface topography. A scanning area of 400 μm^2 (20 μm × 20 μm) was selected to provide detailed mapping of the film morphology.

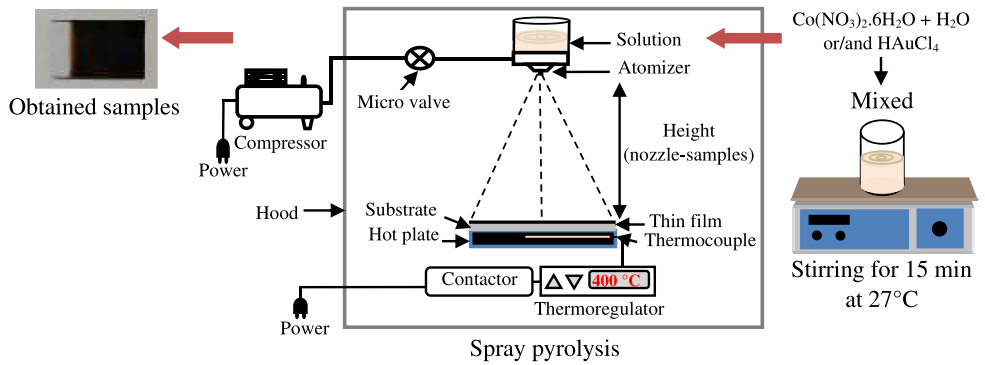

Fig. 1. Schematic diagram of the pneumatic spray technique.

Additionally, the static water contact angle was measured using a 5 μL droplet at room temperature, illuminated by a LEYBOLD light source (6 V, 30 W), to evaluate the wettability of the thin films. Optical properties were further analyzed using a Shimadzu UV-3101 PC spectrophotometer, measuring transmittance across the 300–1000 nm wavelength range, providing critical insights into the films' light-interaction and optical performance. The electrical properties of the films, including resistivity, carrier concentration, and mobility, were evaluated at room temperature using the Van der Pauw method with an Ecopia HMS-3000 Hall effect measurement system. The current–voltage (I–V) characteristics of the heterojunction were analyzed using a Sony Tektronix 370 curve tracer.

3. Results and discussion

3.1. Structural properties

3.1.1. X-ray diffraction findings

Fig. 2 illustrates the X-ray diffraction (XRD) patterns of Co_3O_4 thin films, both pure and doped with varying concentrations of Au (1, 1.5, and 2 wt %). A comparison with the standard JCPDS card no 42–1467 confirms that all samples exhibit a polycrystalline nature with a cubic spinel structure [2,16,17]. The diffractograms reveal multiple prominent diffraction peaks corresponding to the (311), (222) and (400) planes, with the (311) reflection being the most intense and thus indicating a preferred growth orientation along this direction. The increase in the intensity of the (311) diffraction peak observed for Co_3O_4 doped with 1 wt % Au can be attributed to an enhancement of crystallinity and

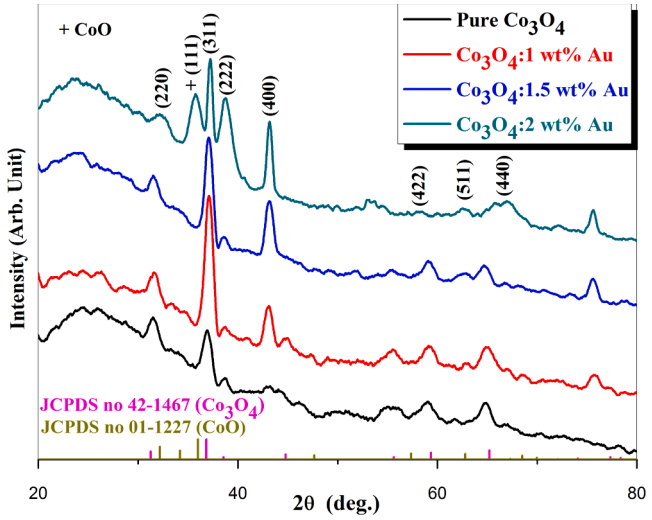

Fig. 2. XRD spectra of Co_3O_4 thin films with different Au concentrations.

a possible reorientation of the preferential growth planes. The incorporation of a small amount of Au^{+3}, which shares the same oxidation state as Co^{+3}, acts as a nucleation facilitator by reducing lattice defects and favoring the formation of larger, well-ordered crystallites. This improvement is directly related to the spinel structure, where Co^{+3} normally occupies octahedral sites (CN = 6); Au^{+3}, when introduced, substitutes at these positions in a coherent manner, thereby stabilizing the lattice and enhancing overall crystallinity. The stronger diffraction intensity associated with this plane therefore reflects an overall improvement in the structural quality of the material at low doping concentrations. Furthermore, when the gold concentration exceeds 1 wt %, an additional peak appears at $2\theta \approx 38.68°$, corresponding to the (222) plane of the Co_3O_4 spinel structure. This emergence can be attributed to localized structural distortions induced by the incorporation of Au^{+3} ions, without altering the dominant crystallographic orientation, which remains centered on the (311) plane. The doping process may thus enhance the visibility of secondary diffraction planes, typically weak, due to lattice strain and increased formation of crystalline defects. As the Au concentration increases beyond the solubility limit ($\geq$ 1.5 wt %), the crystal structure becomes destabilized, leading to the onset of a secondary phase. This is evidenced by the emergence of a peak at $2\theta \approx 35.98°$, which corresponds to the (111) plane of CoO [18] (space group, JCPDS no 01–1227). The formation of this phase may result from a partial reduction of Co_3O_4, where Co^{+3} ions are reduced to Co^{+2}, or from phase separation triggered by excessive Au doping [19]. Similar behavior was reported by Zhang et al. [20] in their investigation of Ni-doped Co_3O_4 thin films, where increasing dopant concentration beyond an optimal level led to a decline in structural quality. Furthermore, a systematic shift of the (311) peak towards higher diffraction angles is observed in all Au-doped samples compared to the pure film (Fig. 3). This rightward shift suggests an apparent contraction of the lattice parameter. This variation can initially be attributed to the incorporation of Au^{+3} ions, whose ionic radius (0.085 nm) is significantly larger than that of Co^{+3} ions (0.0545 nm). Although the substitution of a smaller ion with a larger one would typically lead to lattice expansion, the introduction of these larger ions into the octahedral sites can cause local distortion. To compensate for this local strain, neighboring regions of the crystal may contract, resulting in an overall reduction in the lattice parameter. This internal stress redistribution mechanism may explain the shift toward higher angles observed at low doping levels (1 wt % Au). When the gold concentration exceeds this threshold, a further shift and a broadening of the diffraction peak can also be observed. This behavior suggests the formation of a secondary phase, likely CoO, induced by the oversaturation of the host lattice with Au^{+3} ions. Moreover, the variation in the intensity of the (311) peak observed in the figure can be attributed to differences in crystallite size, which are influenced by the size mismatch between the dopant ions and the atoms in the original crystal structure [21].

This interpretation is further supported by Vesta structural modeling (see Fig. 4), which confirms that pure Co_3O_4 adopts the typical cubic

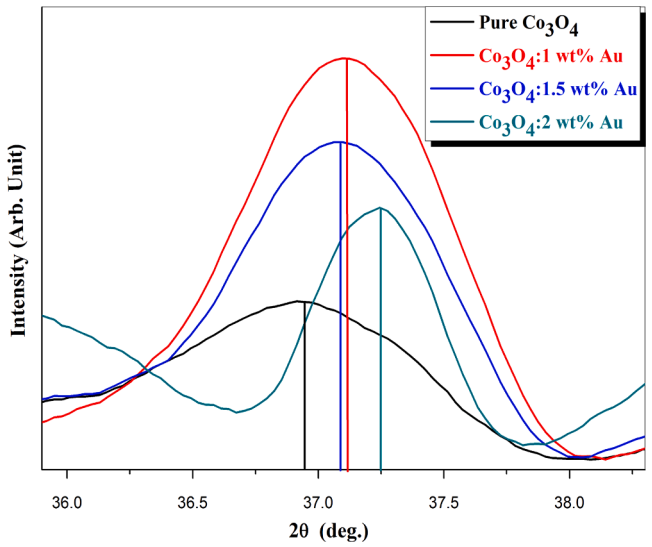

Fig. 3. Zoom of (311) peak positions and intensities of X-ray diffraction of obtained films.

spinel structure (space group *Fd-3 m*), with Co^{+2} ions occupying tetrahedral sites and Co^{+3} ions at octahedral sites, forming a stable and well-ordered framework. In Au-doped samples, the insertion of Au induces local lattice distortions. At low concentration (1 wt %), Au atoms are incorporated either substitutionally or interstitially without disrupting the long-range order, in agreement with the enhanced crystallinity observed in XRD. Conversely, at higher concentrations (1.5–2 wt %), the mismatch between Au and Co ionic radii modifies the Co–O bond environment, increases defect density, and promotes secondary phase formation, consistent with the new diffraction peaks detected.

The average crystallite size (D), microstrain (ε), and dislocation density (δ) of the films were estimated from the dominant (311) diffraction peak using the following equations [8] :

$$D = \frac{0.9\lambda}{\beta\cos\theta} \quad (1)$$

$$\varepsilon = \frac{\beta\cos\theta}{4} \quad (2)$$

$$\delta = \frac{1}{D^2} \quad (3)$$

λ stands for the X-ray's wavelength, β pertains to the full width at half maximum (FWHM) of the diffraction peak, θ indicates the diffraction angle.

Table 1 summarizes the structural parameters, namely the lattice parameter, unit-cell volume, crystallite size, microstrain, and dislocation density, for Co_3O_4 thin films with different Au doping concentrations. The evolution of the lattice parameter and unit-cell volume reveals a non-linear behavior as a function of Au content, in agreement with the XRD results and Vesta modeling. At low doping levels, the incorporation of Au improves the crystallinity and stabilizes the spinel structure without disturbing the long-range order. In contrast, at higher concentrations, the mismatch between the ionic radii of Au and Co leads to local lattice distortions, an increase in defect density, and the formation of a secondary CoO phase. Therefore, low Au doping enhances the structural quality of Co_3O_4, whereas excessive Au incorporation results

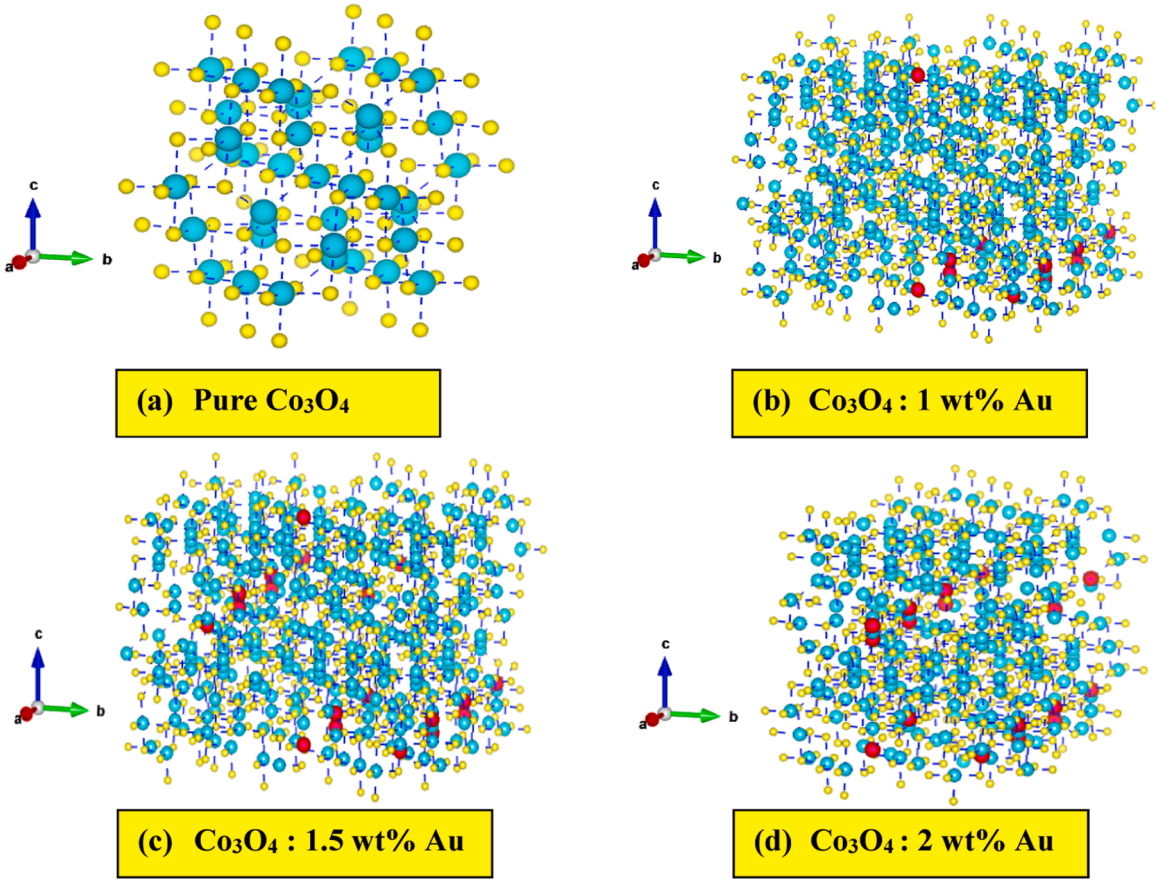

Fig. 4. Structural characterization of pure and Au-doped Co_3O_4: (a) pure Co_3O_4, (b) Co_3O_4:1 % wt Au, (c) Co_3O_4:1.5 % wt Au, and (d) Co_3O_4:2 % wt Au. Atoms are colored as follows: Co (blue), O (yellow), Au (red).

Table 1
Structural parameters of pure Co_3O_4 and Au-doped Co_3O_4 films.

Sample	a, (Å)	V, (Å^3)	d_{311}, (Å)	D, (nm)	ε, (10^{-3})	δ, ($\times10^{-3}$ nm^{-2})	t, (nm)
Pure Co_3O_4	8.054	522.9	2.428	6.34	5.4644	24.88	300
1 wt % Au-Co_3O_4	8.025	517.4	2.419	9.19	3.7711	11.84	508
1.5 wt % Au-Co_3O_4	8.038	519.6	2.423	9.16	3.7835	11.92	421
2 wt % Au-Co_3O_4	8.005	513.0	2.414	6.31	5.4957	25.12	384

in lattice disorder and structural degradation.

According to the same table, it can be observed that as the Au content increases from 0 wt % to 1 wt %, the D increases from 6.34 nm to 9.19 nm. This increase is accompanied by a noticeable reduction in strain and dislocation density, indicating enhanced crystallinity and structural order of the Co_3O_4 films at low doping levels. However, when the gold content exceeds 1 wt %, a decrease in D is observed, indicating a degradation of the films crystalline quality. This degradation in structural quality can be attributed to the partial substitution of Co^{+2} ions (ionic radius ≈ 0.058 nm [22,23]) by Au^{+} ions, which have a larger ionic radius (≈ 0.137 nm [24]). This difference causes significant local distortions in the lattice, leading to internal stresses that disrupt crystalline growth. The excess gold promotes the formation of a secondary CoO phase, which significantly alters the structural parameters of the Co_3O_4 matrix. This secondary phase disrupts the homogeneous growth of crystallites, leading to a reduction in their average size and an increase in defect density, as shown in Table 1. Moreover, the strong lattice mismatch between spinel Co_3O_4 ($a \approx 8.08$ Å) and cubic CoO ($a \approx 4.26$ Å) generates additional internal stress, resulting in higher microstrain (see Table 1). These combined effects degrade the overall crystallinity by enhancing structural disorder and lattice distortions. In addition, they negatively impact the optical and electrical properties, causing lower transparency and higher resistivity. Such observations are consistent with previous reports, where the formation of secondary phases is typically associated with reduced crystallite size, increased defect density, and deterioration of the optoelectronic performance of doped oxides [25]. Similar trends have been documented for other dopants incorporated into Co_3O_4 matrices. Marnadu et al. [5] reported a slight decrease in crystallite size from 8 nm to 7 nm in Co_3O_4 thin films doped with up to 6 wt % Mo, whereas Shkir et al. [8] observed a reduction from 23 nm to 20 nm upon Nd incorporation. Likewise, Fareed et al. [26] recorded a more pronounced decrease from 56 nm to 16 nm with increasing Gd content.

3.1.2. Fourier transform infrared (FTIR) spectra

Fourier Transform Infrared Spectroscopy complements the structural information obtained from XRD. The combined analysis of both techniques provides a more comprehensive understanding of the structure and composition of the deposited films, particularly regarding the nature of the resulting metal oxides. Fig. 5 presents the FTIR transmission spectra of pure cobalt oxide films, as well as those doped with 1, 1.5, and 2 wt % Au, all deposited by spray pyrolysis on glass substrates at 400 °C. As shown in the spectra, characteristic absorption bands of Co_3O_4 are clearly observed in all samples, along with additional bands attributed to O–H stretching vibrations from hydrolyzed compounds. In particular, the O–H stretching band appears around 2930 cm^{-1}. Within the examined spectral range (500–3500 cm^{-1}), all samples exhibit two distinct absorption bands centered at 570 cm^{-1} and 660 cm^{-1}, which are associated with the metal–oxygen (Co–O) stretching vibrations characteristic of the spinel Co_3O_4 structure (space group $Fd\bar{3}m$), as previously reported by Lakehal et al. [27], Ali et al. [28], and Aadil et al. [29]. The

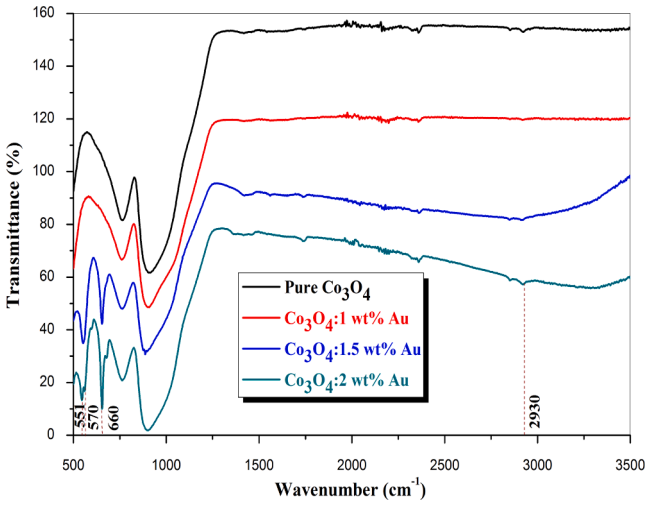

Fig. 5. FTIR spectra of Co_3O_4 thin films as a function of different Au wt % concentrations.

band around 570 cm^{-1} corresponds to the vibration of Co^{+2}-O bonds in the tetrahedral sites, while the band at 660 cm^{-1} is associated with Co^{+3}-O bonds in the octahedral sites of the Co_3O_4 spinel structure. As the gold concentration increases, a new absorption band appears around 551 cm^{-1}, attributed to the stretching vibration of Co^{+2}-O bonds in the tetrahedral sites of the spinel structure. The appearance of this additional band suggests new vibrational modes or specific interactions between gold atoms and the cobalt-oxygen framework, as reported by Abdelhak et al. [3]. When 1 wt % Au is introduced, the peaks become sharper and the intensity slightly increases, indicating homogeneous incorporation of gold without significantly disturbing the Co_3O_4 structure. At a concentration of 1.5 wt % Au, the intensity of the bands decreases, suggesting a modification of the local structure, likely due to lattice distortion caused by the partial substitution of Co^{+2} by Au^{+1}. At 2 wt % Au, the bands become even weaker and slightly broader, indicating further network disturbance, possibly accompanied by the formation of secondary phases, such as CoO [19], or other structural defects. These changes are fully consistent with the XRD results, which also show a progressive distortion of the Co_3O_4 crystal lattice with increasing dopant concentration.

3.2. Surface morphology and wettability analysis

Atomic Force Microscopy (AFM) was employed to investigate the surface topography and roughness of the fabricated Co_3O_4 thin films. Fig. 6 shows the three-dimensional AFM images of nanostructured Co_3O_4 films deposited over a 20 μm × 20 μm scan area, synthesized at 400 °C in open air, as a function of increasing Au doping concentration.

The average surface roughness rises from 28.560 nm for the undoped film to 36.471 nm for the film doped with 1 wt % Au. Interestingly, with further Au doping at 1.5 wt % and 2 wt %, the surface roughness decreases to 32.624 nm and 30.974 nm, respectively. This trend clearly highlights the significant impact of gold incorporation on the surface morphology of the Co_3O_4 thin films. Surface roughness plays a critical role in absorber layers for photovoltaic applications, as it enhances light trapping by introducing irregularities that induce multiple reflections of incident light [10,14]. The light scattering caused by these surface features effectively increases the optical path length, thereby enhancing the overall light absorption capacity of the thin film [10,14]. Furthermore, the distribution of surface peaks and valleys facilitates the internal trapping of more photons within the film structure, amplifying its intrinsic absorption properties and contributing to improved overall optical performance [10,14]. In addition, the AFM results show good agreement with the XRD analyses, particularly regarding the observed

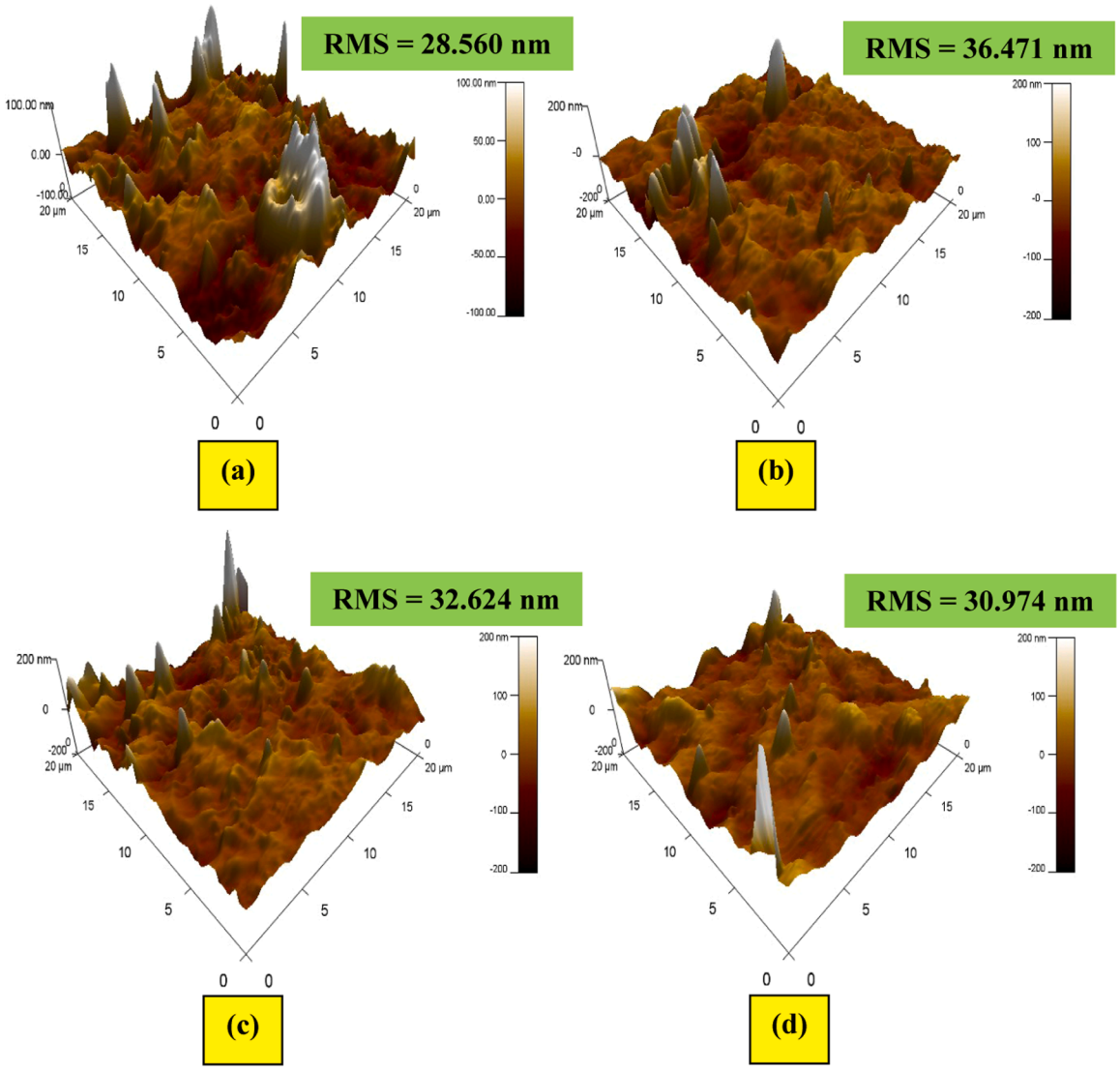

Fig. 6. AFM images of thin films of (a) pure Co_3O_4, (b) 1 wt % Au-Co_3O_4, (c) 1.5 wt % Au-Co_3O_4 and (d) 2 wt % Au-Co_3O_4.

trends in crystallite size evolution.

Fig. 7 presents static water droplets contact angle (CA) images, measured at four different points across the surface of each prepared film. For the Co_3O_4 film doped with 1 wt % Au, the contact angle significantly increases to 101°, compared to 73° for the pure Co_3O_4 film. Notably, the CA value for the 1 wt % Au-doped film exceeds 90°, indicating a hydrophobic surface character [10,30,31]. This hydrophobicity reflects a reduced affinity between the film surface and water droplets, resulting in lower water adhesion. Similar hydrophobic behavior has been documented in previous studies by Nezzari et al. [2] and Darenfad et al. [15], who reported comparable effects in Ni-doped Co_3O_4 and Co-doped CuO thin films, respectively. The hydrophobic nature of the surface is especially beneficial for photovoltaic applications [2,10,15], as it helps reduce moisture-related degradation, thereby enhancing the durability and long-term efficiency of solar devices. The observed increase in contact angle is generally attributed to two main factors: an increase in surface roughness [14] and the growth of crystallite size [32]. In contrast, films doped with higher concentrations of Au (1.5 wt % and 2 wt %) display CA < 90°, indicating a hydrophilic behavior [33]. This transition is consistent with the AFM results shown in Fig. 6, which reveal notable changes in surface morphology as the doping concentration increases. These findings suggest that a 1 wt % Au-doping concentration serves as a critical threshold: beyond this point, significant

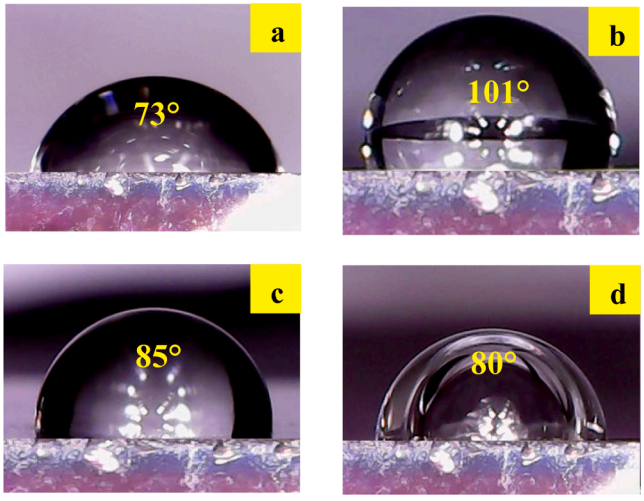

Fig. 7. Water contact angles of (a) pure Co_3O_4, (b) 1 wt % Au-Co_3O_4, (c) 1.5 wt % Au-Co_3O_4 and (d) 2 wt % Au-Co_3O_4.

alterations in the surface structure of Au-doped Co_3O_4 films occur, leading to a marked change in wetting properties. Thus, Au-doped Co_3O_4 films prepared by spray pyrolysis exhibit a remarkable ability to switch between hydrophobic and hydrophilic behavior depending on the gold concentration. This tunable wettability provides valuable flexibility for tailoring the surface properties of the films to specific applications. The findings indicate that a 1 wt % Au-doping level serves as a critical point, where significant modifications in surface state occur, closely associated with variations in roughness and crystallization dynamics during the film growth process.

3.3. Optical properties

UV–Vis measurements were carried out between 300 and 900 nm to investigate the optical properties of our films. The UV–visible spectra of the pure Co_3O_4 films and those doped with gold (1, 1.5, and 2 wt %) are shown in Fig. 8. The evolution of optical transmittance in the Au-doped Co_3O_4 thin films displays a non-linear trend with increasing Au concentration: a sharp decrease to 2.40 % is observed at 1 wt % Au, followed by a gradual rise between 1.5 wt % and 2 wt % Au. This behavior can be explained by the combined effects of structural modifications and changes in surface coloration induced by doping. At 1 wt % Au, the significant reduction in transmittance is mainly attributed to the considerable increase in film thickness (Table 1) and roughness (Fig. 6), which enhances light absorption. Thicker films naturally absorb more light, while the presence of larger crystallites promotes a denser crystal lattice, further boosting absorption. Similar behavior has been reported by Nezzari et al. [2], who studied Ni-doped Co_3O_4 thin films prepared by spray pyrolysis, and by Alem et al. [34], who investigated pure and Ag-doped Co_3O_4 films synthesized by the co-precipitation method. In contrast, at higher Au concentrations (1.5 – 2 wt %), transmittance increases, likely due to a concurrent reduction in film thickness, which decreases overall absorption. The transmission spectra exhibit a general profile characterized by two absorption regions: one between 400 – 550 nm and another between 650 – 800 nm, corresponding to charge transfer transitions of ($O^{-2} \rightarrow Co^{+2}$) and ($O^{-2} \rightarrow Co^{+3}$) in Co_3O_4, respectively. Previous reports [16,17,27], suggest these features indicate the presence of two distinct band gaps. With varying Au concentrations, different absorption bands appear. Using Tauc's method [2,16,17], two energy band gaps were identified, reflecting the electronic band structure of cobalt oxide. The band gap energies were estimated by extrapolating the linear regions of the absorption curves to the point where absorption becomes zero ($\alpha = 0$), as illustrated in Fig. 9. The presence of two distinct band gaps observed in this Figure can be attributed to the electronic band structure of Co_3O_4. The first band gap (Eg_1) is associated with charge transfer from O^{-2} to Co^{+3}, whose energy level lies just below the conduction band. The second, wider band gap (Eg_2), corresponds to the $O^{-2} \rightarrow Co^{+2}$ transition and is considered the fundamental band gap of Co_3O_4 [10]. This dual-gap feature comprising both direct and indirect transitions offers a significant advantage for Co_3O_4 as an absorber layer, enabling effective light absorption across a wide spectral range that includes both the visible and near-infrared regions. Such optical behavior enhances solar energy harvesting, making Co_3O_4 highly promising for photovoltaic applications.

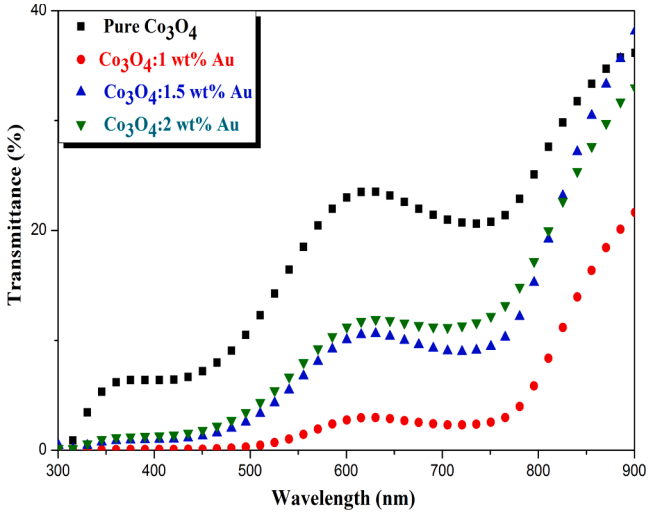

Fig. 8. Transmission spectra for Au doped Co_3O_4 thin films.

The band gap (Eg) of pure nanocrystalline Co_3O_4 was initially measured at 1.41 eV and 2.09 eV. Upon doping with 1 wt % Au, these values increased slightly to 1.48 eV and 2.14 eV, respectively. However, as the Au concentration increased further, the band gap values began to decrease. A similar trend was reported by Muradov et al. [35], who observed that the band gap of pure Co_3O_4 nanoparticles, initially 1.58 eV and 3.33 eV, rose to 1.70 eV and 3.43 eV with 2 % Cu doping. However, when the Cu content was increased to 4 %, 6 %, and 10 %, the band gap gradually decreased. The initial increase in the Eg for Co_3O_4 thin films doped with 1 wt % Au can be attributed to the Moss-Burstein effect. This phenomenon occurs when the Fermi level shifts into the conduction band, effectively widening the energy band gap [35]. A similar enhancement of both Eg_1 and Eg_2 was reported by Saad et al. [36], who studied the effect of 3 % Li and/or 3 % Na doping in Co_3O_4 films prepared by spin-coating. This increase in defects introduces localized states within the band gap, which can reduce the effective band gap energy. The reduction in the Eg can be attributed to two factors: (i) the formation of defect levels within the band gap due to variations in the doping ratio, as reported by Güneri [37]; and (ii) the formation of a secondary CoO phase, which possesses a narrower intrinsic band gap ranging from 0.7 to 1.1 eV, thereby contributing to the overall reduction in the observed energy band gap [38]. Notably, the calculated band gap values fall within a suitable range for photovoltaic applications, making these films promising as absorber layers [39,40]. In particular, the Co_3O_4 film doped with 1 wt % Au demonstrates optimal band gap characteristics for solar cell use, as it closely matches the solar spectrum, thereby enhancing light absorption and improving the efficiency of energy conversion (Fig. 10).

3.4. Electrical properties

The electrical properties of pure and Au-doped Co_3O_4 thin films were analyzed at room temperature using the Hall effect technique. The electrical resistivity (ρ), Hall mobility (μ), and charge carrier concentration (n) are summarized in Table 2. The positive sign of the Hall coefficient confirms that all samples exhibit p-type conduction [10]. As shown in the table, introducing 1 wt % Au leads to a significant drop in resistivity, from 2.346 Ω.cm for pure Co_3O_4 to 6.915×10^{-1} Ω.cm. This reduction is primarily attributed to an increase in charge carrier concentration (Table 2) and may also result from a denser microstructure, which provides more active sites for redox reactions and facilitates charge transport [41]. Moreover, since Au^{+3} has the same valence as Co^{+3}, it does not directly create charge carriers. However, it can improve the crystal structure and reduce defects (as shown in Table 1), particularly oxygen vacancies, which decreases carrier trapping and thus enhances the resistivity. Likewise, Bhargava et al. [42] reported that optimal Mn doping in Co_3O_4 films enhanced carrier mobility and thereby improved conductivity. Additionally, Darenfad et al. [14,15] noted that the hydrophobic nature of absorber films contributes to better electrical properties. This is supported by the contact angle measurement of 95° for the 1 wt % Au-doped film (Fig. 7). However, when the Au content reaches or exceeds 1.5 wt %, resistivity begins to increase again, likely due to a decline in crystalline quality, as suggested by Table 1. A comparable trend was observed by Nezzari et al. [2] in Ni-doped films at 4 % and 6 % concentrations. This rise in resistivity may stem from several factors: (i) a shift toward hydrophilic behavior [14]; (ii) a

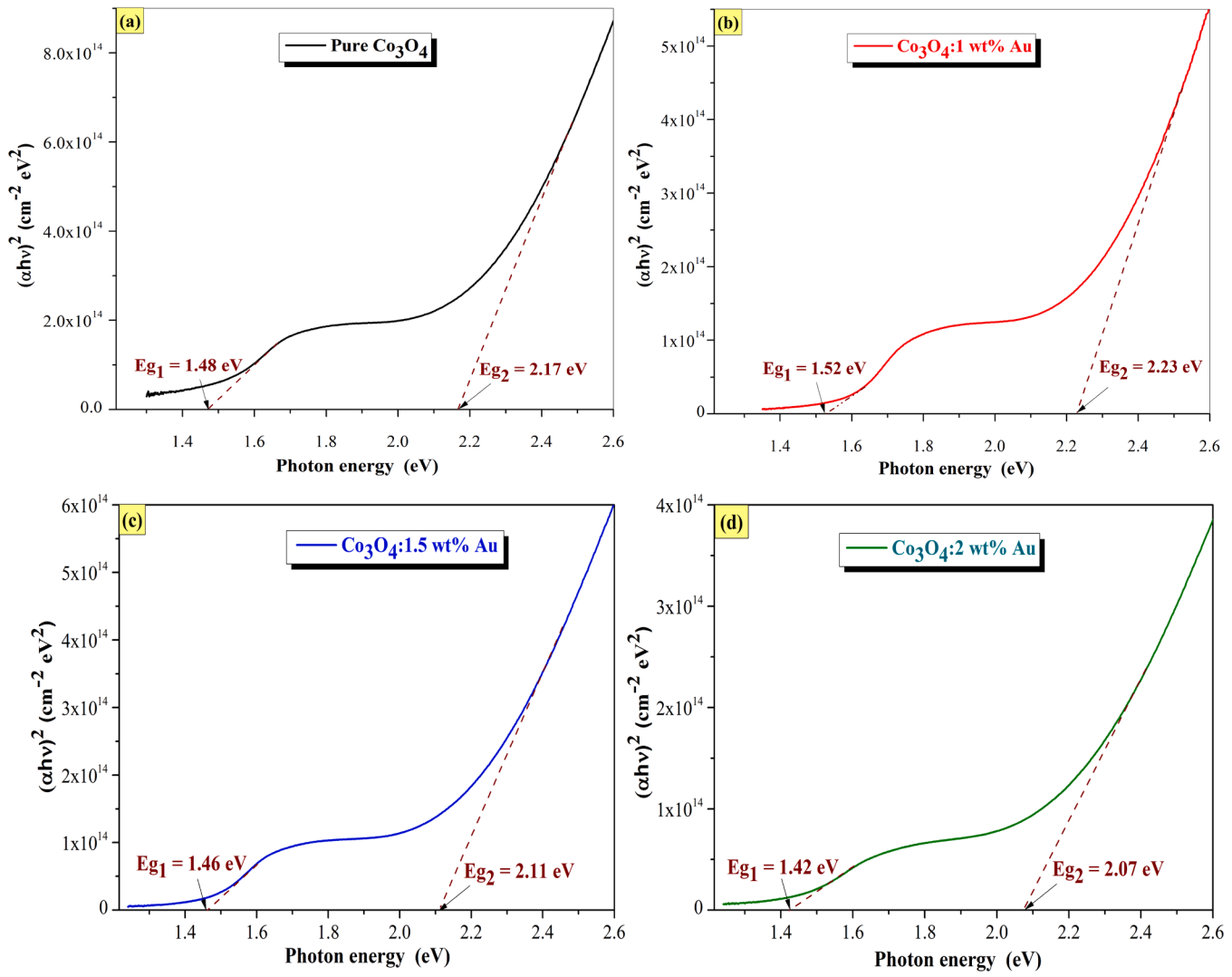

Fig. 9. Tauc's plot of (a) pure Co_3O_4, (b) Co_3O_4: 1 wt % Au, (c) Co_3O_4: 1.5 wt % Au, and (d) Co_3O_4: 2 wt % Au thin films.

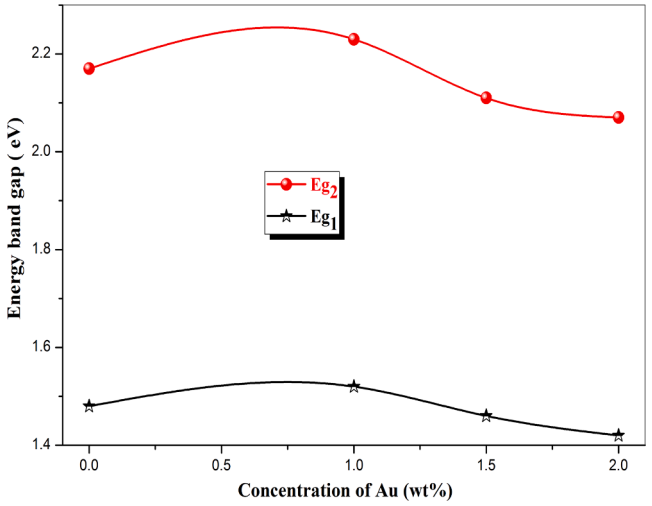

Fig. 10. Variation of the two energy band gaps E_{g1} and E_{g2} of Au-doped Co_3O_4 thin films.

Table 2
Electrical resistivity, Hall mobility and carriers concentration of pure and Au-doped Co_3O_4 films.

Sample	Resistivity, (Ω.cm)	Hall mobility, (cm^2/Vs)	Carrier concentration, (cm^{-3})
Pure Co_3O_4	28.39	1.633×10^{-2}	6.581×10^{16}
1 wt % Au-Co_3O_4	0.6915	6.302	1.433×10^{18}
1.5 wt % Au-Co_3O_4	2.92	3.77×10^{-1}	5.66×10^{17}
2 wt % Au-Co_3O_4	5.267	1.9×10^{-1}	1.36×10^{16}

reduction in charge carrier (hole) density, possibly due to compensation effects or interactions between dopant atoms and the host lattice, limiting the availability of carriers for conduction [2]; (iii) decreased carrier mobility resulting from increased scattering by dopant-induced defect centers; and (iv) a reduction in adsorbed oxygen at the film surface, which negatively affects surface charge transfer processes.

Fig. 11 illustrates the variation in both crystallite size and charge carrier mobility of Co_3O_4 thin films as a function of Au doping concentration. The incorporation of Au as a dopant in Co_3O_4 thin films exhibits a non-linear effect on both the crystallite size and the charge carrier mobility, characterized by an initial increase up to 1 wt % Au, followed by a decrease at higher doping levels (1.5 – 2 wt % Au). At low Au concentrations ($\leq$ 1 wt %), Au^{+3} ions effectively substitute for Co^{+3} ions within the Co_3O_4 lattice, leading to a reduction of intrinsic defects

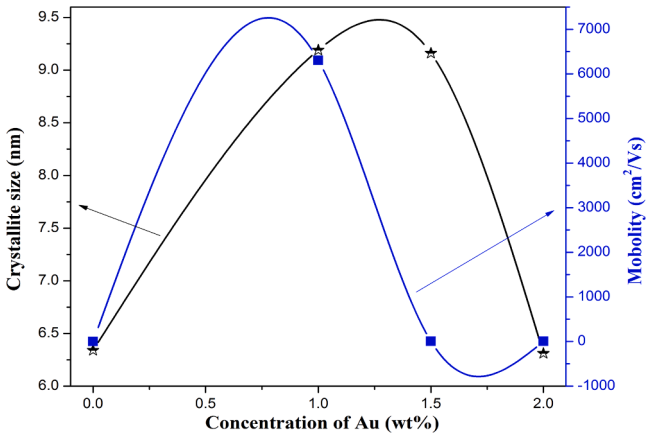

Fig. 11. Variations of crystallite size and mobility of our films.

such as dislocations and vacancies. This structural improvement facilitates crystallite growth, resulting in larger grain sizes and fewer grain boundaries. Consequently, the charge carriers experience fewer scattering centers, leading to enhanced carrier mobility. However, beyond the optimal doping threshold (~1–1.5 wt % Au), the lattice reaches saturation, and excess Au tends to accumulate at grain boundaries or segregate into secondary phases. This leads to the formation of structural distortions and additional defect states, including metallic Au clusters or over-substitutional stress, which disrupts the crystalline order. As a result, the crystallite size decreases due to inhibited grain coalescence, and the density of scattering and recombination centers increases, ultimately reducing the carrier mobility. Therefore, the parallel evolution of D and carrier mobility as a function of Au doping is governed by the balance between defect reduction at low doping levels and defect generation at high doping levels, highlighting the existence of an optimal doping concentration for maximizing both structural and electronic performance.

In this study, a thin-film heterojunction was successfully fabricated by integrating an n-type ZnO layer with a p-type Co_3O_4 layer doped with 1 wt % gold, as illustrated in Fig. 12. Fig. 13 presents the current–voltage (I–V) characteristic of the 1 wt % Au-Co_3O_4/ZnO/FTO/Glass heterojunction. The I–V analysis provides essential insights into the diode junction parameters, including the series resistance (R_s), ideality factor (n), and reverse saturation current (I_s). These parameters can be extracted using the following equation [11]:

$$I(V) = I_s\left(\exp\left(\frac{qV}{kTn}\right) - 1\right) \tag{4}$$

Where k is Boltzmann constant, T the absolute temperature and q the elementary electronic charge.

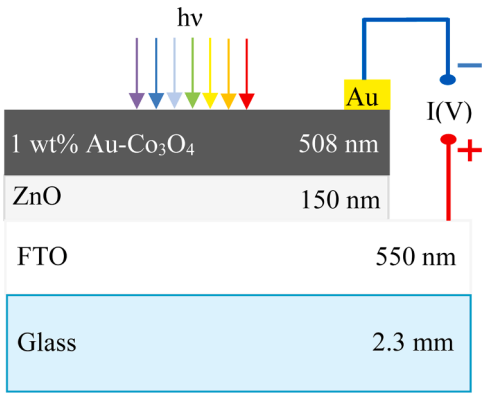

Fig. 12. Diagram of 1 wt % Au-Co_3O_4/ZnO/FTO/Glass solar cell structure.

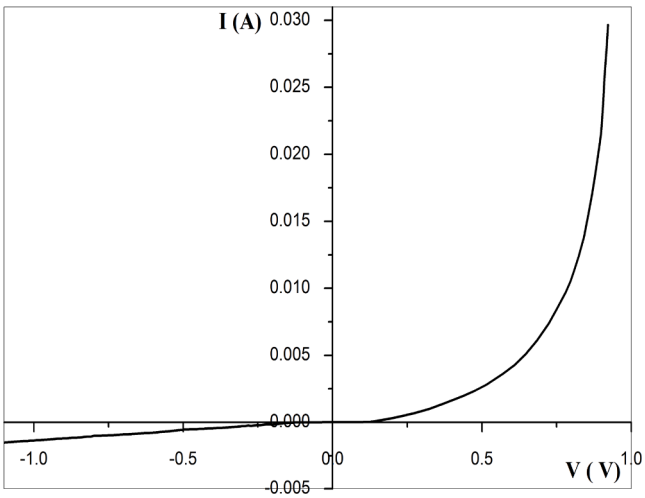

Fig. 13. I(V) characteristic of the 1 wt % Au-Co_3O_4/ZnO/FTO heterojunction.

The ideality factor is determined from the slope of the linear region in the forward bias of the I–V curve and is calculated using the following equation [11]:

$$n = \frac{q}{kT}\left(\frac{dV}{d(\ln I)}\right) \tag{5}$$

The obtained value of the ideality factor is $n = 1.65$ (see Table 3). This value ($1 < n < 2$) indicates that, in addition to the ideal diffusion current, trap-assisted recombination in the space-charge region [7]. Consequently, the observed non-idealities are most likely associated with microstructural defects, localized states induced by doping, and interface disorder. Such ideality factor values are typically reported for oxide-based thin-film junctions, where recombination processes dominate charge transport over pure diffusion. In parallel, the extracted series resistance is relatively low ($R_s = 6.57\ \Omega$), which reflects good conduction across the junction and limits ohmic losses. The measured reverse saturation current $I_s = 2.37 \times 10^{-4}$ A, a value consistent with oxide-based heterojunctions, indicating a satisfactory rectifying behavior but still affected by non-ideal recombination processes. Overall, these results suggest that the junction exhibits promising potential for photovoltaic applications; however, further optimization to minimize defects and trap states is required to enhance the overall power conversion efficiency.

Table 4 presents a comparative summary of the structural, optical, electrical, and heterojunction parameters of various doped Co_3O_4 thin films reported in the literature, along with the present results obtained for Au:Co_3O_4 films. All the investigated systems exhibit a typical spinel cubic structure with band gap energies lying in the range of 1.2–2.6 eV, which is consistent with the semiconducting nature of Co_3O_4. In terms of electrical properties, Au– Co_3O_4 films exhibit a resistivity of 6.9×10^{-1} Ω.cm, significantly lower than that of pure Co_3O_4 (7.94 Ω.cm). Regarding heterojunction behavior, the p–Au:Co_3O_4/n–ZnO junction fabricated in this work shows an ideality factor of 1.65, lower than those reported for other Co_3O_4-based systems such as p-Mo:Co_3O_4/n–Si (n = 2.3) and p-Sn:Co_3O_4/n–Si (n = 3.7). This value, close to unity, indicates a better interfacial quality with fewer recombination centers and more efficient charge transfer across the junction interface. Overall, the Au:Co_3O_4thin films combine favorable optical and electrical properties with improved heterojunction performance, confirming that Au doping

Table 3
Electrical parameters of the 1 wt %Au-Co_3O_4/ZnO/FTO heterojunction.

Structure	R_s, (Ω)	N	I_s, (A)
1 wt % Au-Co_3O_4/ZnO/FTO	6.57	1.65	2.37×10^{-4}

Table 4
Comparative structural, optical, electrical, and heterojunction parameters reported for various doped Co_3O_4 thin films, including the present Au:Co_3O_4 films.

Materials type	a, (Å)	UV–Vis Band gap value, eV	Resistivity, Ω.cm	heterojunction	n	Ref.
Pure Co_3O_4	-	$Eg_1 = 1.27$	7.94	Co_3O_4/ZnO/FTO	1.64	[17]
Ni-Co_3O_4	-	$Eg_1 = 1.3–1.41$ $Eg_2 = 1.99–2.09$	1.78×10^{-1}	-	-	[2]
Mo-Co_3O_4	8.148	$Eg_1 = 1.49–1.55$ $Eg_2 = 2.03–2.15$	-	p-Mo@Co_3O_4/n-Si	2.3	[5]
Sn-Co_3O_4	-	$Eg_2 = 2.1–2.6$	-	p-Sn@Co_3O_4/n-Si	3.7	[7]
Nd-Co_3O_4	8.085	$Eg_1 = 1.49–1.55$ $Eg_2 = 2.03–2.15$	-	-	-	[8]
Cu-Co_3O_4	-	-	-	p-Cu:Co_3O_4/n-Si	1.24	[43]
Cr-Co_3O_4	8.109	$Eg_2 = 1.95–2.1$	4.7×10^{-1}	-	-	[44]
Au-Co_3O_4	8.025	$Eg_1 = 1.42–1.48$ $Eg_2 = 2.07–2.17$	6.915×10^{-1}	p-Au:Co_3O_4/n-ZnO	1.65	This work

effectively tunes the electronic structure and enhances the functional potential of Co_3O_4 for optoelectronic and photovoltaic device applications.

4. Conclusions

Single-phase spinel cubic Co_3O_4 thin films doped with gold were successfully synthesized via the chemical spray pyrolysis method, exhibiting crystallite sizes in the range of 6.31–9.19 nm. X-ray diffraction confirmed that all films were polycrystalline with a cubic spinel structure and showed a preferred orientation along the (311) plane. However, with increasing Au content, the appearance of a secondary CoO phase was detected in both the XRD and FTIR spectra. AFM revealed that the surface morphology was strongly dependent on the gold concentration. The 1 wt % Au–doped Co_3O_4 film displayed the highest surface roughness, corresponding to a more textured surface compared to the undoped and other doped samples. Static contact angle measurements confirmed the hydrophobic nature of this film, with a contact angle exceeding 90°, which is advantageous for thin-film solar cell applications. Optical transmittance spectra showed that the hydrophobic 1 wt % Au– Co_3O_4 film exhibited reduced transparency in the 300–800 nm wavelength range relative to the more transparent, hydrophilic films. Optical band gap analysis revealed two direct transitions, Eg_1 and Eg_2, which slightly decreased from 1.48 eV to 1.42 eV and from 2.17 eV to 2.07 eV, respectively, with increasing Au content. Electrical measurements demonstrated that the 1 wt % Au– Co_3O_4 film exhibited improved electrical performance, characterized by a low resistivity (6.915×10^{-1} Ω.cm) and a high carrier concentration (1.433×10^{18} cm^{-3}). Moreover, the fabricated n–ZnO/p–Co_3O_4 heterojunction displayed a clear rectifying behavior, confirming its potential for photovoltaic applications. Overall, the incorporation of 1 wt % Au into Co_3O_4 provided the optimal balance between structural enhancement, hydrophobic surface properties, and electrical conductivity, yielding an ideality factor of 1.65. This composition thus appears to be the most promising for optoelectronic and solar cell applications.

Funding

This work is supported by the Research Project University-Formation (PRFU) of Algerian ministry of high education and scientific research (no A10N01UN280120220009). The project, titled 'Study, elaboration and characterization of the effect of doping and co-doping on the properties of oxides of transition metals for optoelectronic applications'.

CRediT authorship contribution statement

Warda Darenfad: Writing – review & editing, Writing – original draft, Validation, Methodology, Investigation, Funding acquisition, Formal analysis, Data curation, Conceptualization. **Younes Nezzari:** Writing – original draft, Visualization, Validation, Software, Resources, Investigation, Formal analysis, Data curation. **Noubeil Guermat:** Visualization, Validation, Software, Resources, Project administration, Methodology, Investigation. **Kamel Mirouh:** Visualization, Validation, Software, Resources, Methodology, Investigation, Formal analysis. **Nadir Bouarissa:** Validation, Supervision, Resources, Project administration, Funding acquisition, Formal analysis, Data curation, Conceptualization. **Amor Azizi:** Visualization, Validation, Project administration, Methodology, Investigation, Data curation.

Declaration of competing interest

The authors declare that they have no known competing financial interests or personal relationships that could have appeared to influence the work reported in this paper.

Data availability

No data was used for the research described in the article.

References

[1] P. Cheng, F. Dang, Y. Wang, J. Gao, L. Xu, C. Wang, L. Lv, X. Li, B. Zhang, B. Liu, Gas sensor towards n-butanol at low temperature detection: hierarchical flower-like Ni-doped Co_3O_4 based on solvent-dependent synthesis, Sens. Actuat. B: Chem. 328 (2021) 129028, https://doi.org/10.1016/j.snb.2020.129028.
[2] Y. Nezzari, W. Darenfad, K. Mirouh, N. Guermat, N. Bouarissa, R. Merah, Hydrophobic nickel doped Co_3O_4 sprayed thin films as solar absorber, Opt. Quant. Electron 56 (2024) 951, https://doi.org/10.1007/s11082-024-06930-6.
[3] L. Abdelhak, B. Amar, B. Bedhiaf, D. Cherifa, B. Hadj, Characterization of Mn-doped Co_3O_4 thin films prepared by sol gel-based dip-coating process, High. Temp. Mater. Process. 38 (2019) 237–247, https://doi.org/10.1515/htmp-2017-0185.
[4] N. Zhang, Q. Qin, X. Ma, J. Zhou, L. Sun, C. Chen, S. Wen, Y. Chen, S. Ruan, One-step synthesis and gas sensing properties of hierarchical Fe doped Co_3O_4 nanostructures, J. Alloy. Compd. 723 (2017) 779–786, https://doi.org/10.1016/j.jallcom. 2017.06.301.
[5] R. Marnadu, M. Shkir, J. Hakami, I.M. Ashraf, P. Baskaran, D. Sivaganesh, K. V. Chandekar, W.K. Kim, S. Gedi, Significant enhancement in photosensitivity, responsivity, detectivity and quantum efficiency of Co_3O_4 nanostructured thin film-based photodetectors through Mo doping developed by spray pyrolysis method, Surf. Interface. 34 (2022) 102366, https://doi.org/10.1016/j.surfin.2022.102366.
[6] C. Dalache, H. Benhebal, B. Benrabah, A. Ammari, A. Kharroubi, A. Lakhal, Cadmium-doped Co_3O_4 thin films: synthesis and characterization, Surf. Rev. Lett. 26 (2019) 1–9, https://doi.org/10.1142/S0218625×18501342.
[7] H. Albargi, R. Marnadu, G. Sujithkumar, A.S. Alkorbi, H. Algadi, M. Shkir, A. Umar, G. Sreedevi, Deposition of nanostructured Sn doped Co_3O_4 films by a facile nebulizer spray pyrolysis method and fabrication of p-Sn doped Co_3O_4/n-Si junction diodes for opto-nanoelectronics, Sens. Actuat. A Phys. 332 (2021) 113067, https://doi.org/10.1016/j.sna.2021.113067.
[8] M. Shkir, A. Khan, M. Imran, M.A. Khan, R.A. Zargar, T. Alshahrani, K. Deva Arun Kumar, P. Mohanraj, K.V. Chandekar, S. AlFaify, Spray pyrolysis developed Nd doped Co_3O_4 nanostructured thin films and their structural, and opto-nonlinear properties for optoelectronics applications, Opt. Laser Technol. 150 (2022) 107959, https://doi.org/10.1016/j.optlastec.2022.107959.
[9] B. Wang, X. Zhu, S. Li, M. Chen, N. Liu, H. Yang, M. Ran, H. Lu, Y. Yang, Enhancing the photovoltaic performance of perovskite solar cells using plasmonic Au@Pt@Au core-shell nanoparticles, Nanomaterials 9 (2019) 1263, https://doi.org/10.3390/nano9091263.
[10] Y. Nezzari, W. Darenfad, K. Mirouh, N. Guermat, N. Bouarissa, Structural, wettability, optical, and electrical modifications by varying precursor solutions of sprayed Co_3O_4 thin films for solar cell applications, Eur. Phys. J. B 98 (2025) 44, https://doi.org/10.1140/epjb/s10051-025-00889-3.

[11] R. Merah, W. Darenfad, K. Mirouh, N. Guermat, N. Bouarissa, A comparative study on the optoelectronic properties of $BiFeO_3$ and $BiMnO_3$ sprayed thin films as solar absorbers, Phys. B: Condens. Matter 715 (2025) 417566, https://doi.org/10.1016/j.physb.2025.417566.

[12] I. Bellili, W. Darenfad, N. Guermat, N. Bouarissa, Optimizing the structural, optical, hydrophobic, and electrical properties of (Sn/Mg) co-doped ZnO thin films for application as solar cell electrodes, J. Mater. Sci. Mater. Electron. 36 (2025) 872, https://doi.org/10.1007/s10854-025-14918-5.

[13] W. Darenfad, N. Guermat, K. Mirouh, Thoughtful investigation of ZnO doped Mg and co-doped Mg/Mn, Mg/Mn/F thin films: a first study, J. Mol. Struct. 1286 (2023) 135574, https://doi.org/10.1016/j.molstruc.2023.135574.

[14] W. Darenfad, N. Guermat, K. Mirouh, Deposition time dependent physical properties of semiconductor CuO sprayed thin films as solar absorber, Eur. Phys. J. Appl. Phys. 99 (2024) 17, https://doi.org/10.1051/epjap/2024230200.

[15] W. Darenfad, N. Guermat, K. Mirouh, Effect of Co-doping on structural, morphological, optical and electrical properties of p-type CuO films, J. Nano-Electron. Phys. 15 (06) (2023) 06009, https://doi.org/10.21272/jnep.15(6).06009.

[16] W. Daranfed, N. Guermat, K. Mirouh, Experimental study in the effect of precursors in Co_3O_4 thin films used as solar absorbers, Ann. Chim. -Sci Mat. 44 (2020) 121–126, https://doi.org/10.18280/acsm.440207.

[17] W. Darenfad, N. Guermat, N. Bouarissa, F.Z. Satour, A. Zegadi, K. Mirouh, Improvement in optoelectronics and photovoltaic properties of p-Co_3O_4/n-ZnO hetero-junction: effect of deposition time of sprayed Co_3O_4 thin films, J. Mater. Sci. Mater. Electron. 35 (2024) 162, https://doi.org/10.1007/s10854-023-11909-2.

[18] N. Joshi, S.A. Shivashankar, R. Narayan, Surfactant-free synthesis and magnetic property evaluation of air-stable cobalt oxide nanostructures, Nano Express 4 (2023) 035009, https://doi.org/10.1088/2632-959X/acf4ae.

[19] M. Lim, Z. Ma, G. O'Connell, J.A. Yuwono, P. Kumar, R. Jalili, R. Amal, R. Daiyan, E.C. Lovell, Ru-induced defect engineering in Co_3O_4 lattice for high performance electrochemical reduction of nitrate to ammonium, Small 20 (2024) 2401333, https://doi.org/10.1002/smll.202401333.

[20] Y. Zhang, C. Huang, J. Lu, H. Cao, C. Zhang, X.S. Zhao, Ni-modified Co_3O_4 with competing electrochemical performance to noble metal catalysts in both oxygen reduction and oxygen evolution reactions, Appl. Surf. Sci. 651 (2024) 159241, https://doi.org/10.1016/j.apsusc.2023.159241.

[21] M. Kaur, V. Kumar, J. Singh, J. Datt, R. Sharma, Effect of Cu-N co-doping on the dielectric properties of ZnO nanoparticles, Mater. Technol. 37 (2022) 2644–2658, https://doi.org/10.1080/10667857.2022.2055909.

[22] I. Bellili, M. Mahtali, W. Darenfad, N. Guermat, The figure of merit improvement of (Sn, Co)–ZnO sprayed thin films for optoelectronic applications, Opt. Mater. 154 (2024) 115785, https://doi.org/10.1016/j.optmat.2024.115785.

[23] W. Darenfad, N. Guermat, N. Bouarissa, K. Mirouh, Investigation of structural, morphological and optoelectronic properties of (Ni, Co)-doped and (Ni/Co) co-doped SnO_2 (110) sprayed thin films, J. Mol. Struct. 1317 (2024) 138992, https://doi.org/10.1016/j.molstruc.2024.138992.

[24] Z.Q. Jiang, G. Yao, X.Y. An, Y.J. Fu, L.H. Cao, W.D. Wu, X.M. Wang, Electronic and optical properties of Au-doped Cu_2O: a first principles investigation, Chin. Phys. B 23 (2014) 057104, https://doi.org/10.1088/1674-1056/23/5/057104.

[25] A. Khalaf, A. Aridi, D. Dasuki, M. Elkady, K. Habanjar, G.M. El-Subruiti, R. Awad, Impact of various dopants (X = Zn, Mg, and Bi) on the structural, optical, and adsorption properties of $(Co_{0.8}Ni_{0.1}X_{0.1})_3O_4$ nanostructures, Sci. Rep. 15 (2025) 26326, https://doi.org/10.1038/s41598-025-10965-4.

[26] S. Fareed, R. Medwal, J.V. Vas, I.A. Khan, R.S. Rawat, M.A. Rafiq, Tailoring oxygen sensing characteristics of Co_3O_4 nanostructures through Gd doping, Ceram. Int. 46 (7) (2020) 9498–9506, https://doi.org/10.1016/j.ceramint.2019.12.211.

[27] A. Lakehal, B. Bedhiaf, A. Bouaza, H. Benhebal, A. Ammaric, C. Dalache, Structural, optical and electrical properties of Ni-doped Co_3O_4 prepared via Sol-Gel tech nique, Mat. Res. 21 (2018) 20170545, https://doi.org/10.1590/1980-5373-MR-2017-0545.

[28] G.A.M. Ali, O.A. Fouad, S. Makhlouf, Structural, optical and electrical properties of sol-gel prepared mesoporous Co_3O_4/SiO_2 nanocomposites, J. Alloy. Compd. 579 (2013) 606–611, https://doi.org/10.1016/j.jallcom.2013.07.095.

[29] M. Aadil, S. Zulfiqar, M. Shahid, S. Haider, I. Shakir, M. Farooq Warsi, Binder free mesoporous Ag-doped Co_3O_4 nanosheets with outstanding cyclic stability and rate capability for advanced supercapacitor applications, J. Alloy. Compd. 844 (2020) 156062, https://doi.org/10.1016/j.jallcom.2020.156062.

[30] Z. Belamri, W. Darenfad, N. Guermat, Molarity dependence of solution on structural and hydrophobic properties of ZnO nanostructures, Eur. Phys. J. Appl. Phys. 99 (2024) 10, https://doi.org/10.1051/epjap/2024230146.

[31] Z. Belamri, W. Darenfad, N. Guermat, Impact of annealing temperature on surface reactivity of ZnO nanostructured thin films deposited on aluminum substrate, J. Nano- Electron. Phys. 15 (2023) 02026, https://doi.org/10.21272/jnep.15(2).02026.

[32] N. Guermat, W. Darenfad, K. Mirouh, N. Bouarissa, M. Khalfallah, A. Herbadji, Effects of zinc doping on structural, morphological, optical and electrical properties of SnO_2 thin films, Eur. Phys. J. Appl. Phys. 97 (2022) 14, https://doi.org/10.1051/epjap/2022210218.

[33] M. Khalfallah, N. Guermat, W. Daranfed, N. Bouarissa, H. Bakhti, Hydrophilic nickel doped porous SnO_2 thin films prepared by spray pyrolysis, Phys. Scr. 95 (2020) 095805, https://doi.org/10.1088/1402-4896/aba8c5.

[34] A.F. Alem, A.K. Worku, D.W. Ayele, T.A. Wubieneh, A.A. Teshager, T.M. Kndie, B. T. Admasu, M.A. Teshager, A.A. Asege, M.D. Ambaw, M.A. Zeleke, A.K. Shibesh, T. A. Yemata, Ag doped Co_3O_4 nanoparticles for high-performance supercapacitor application, Heliyon 9 (2023) e13286, https://doi.org/10.1016/j.heliyon.2023.e13286.

[35] M.B. Muradov, S.J. Mammadyarova, G.M. Eyvazova, O.O. Balayeva, G. Aliyeva, I. Hasanova, S.Z. Melikova, N. Musayeva, N. Sadigov, M.I. Abdullayev, Synthesis of $Cu_xCo_{3-x}O_4$ nanoparticles by a sonochemical method and characterization of structural and optical properties and photocatalytic activity for the degradation of methylene blue, RSC Adv. 14 (2024) 1082–1093, https://doi.org/10.1039/D2RA08060E.

[36] R. Saad, K. Abdelkarem, A.M. El Sayed, M. Shaban, I.A. Ahmed, M.T. Tammam, H. Hamdy, Characterization and enhanced carbon dioxide sensing performance of spin-coated Na- and Li-doped and Co-doped cobalt oxide thin films, RSC Adv. 14 (2024) 36852–36867, https://doi.org/10.1039/d4ra06847e.

[37] E. Güneri, The role of Au doping on the structural and optical properties of Cu_2O films, J. Nano Res. 58 (2019) 49–67, https://doi.org/10.4028/www.scientific.net/JNanoR.58.49.

[38] Y. Wang, H.X. Ge, Y.P. Chen, X.Y. Meng, J. Ghanbaja, D. Horwat, J.F. Pierson, Wurtzite CoO: a direct band gap oxide suitable for a photovoltaic absorber, Chem. Commun. 54 (2018) 13949–13952, https://doi.org/10.1039/C8CC06777E.

[39] B. Kupfer, K. Majhi, D.A. Keller, Y. Bouhadana, S. Rühle, H.N. Barad, A. Y. Anderson, A. Zaban, Thin film Co_3O_4/TiO_2 heterojunction solar cells, Adv. Energy Mater. 5 (2015) 1401007, https://doi.org/10.1002/aenm.201401007.

[40] C.T. Ho, T.H. Weng, C.Y. Wang, S.J. Yen, T.R. Yew, Tunable band gaps of $Co_{3-x}Cu_xO_4$ nanorods with various Cu doping, RSC Adv. 4 (2014) 20053–20057, https://doi.org/10.1039/C4RA01463D.

[41] J. Wang, H. Zhang, H. Duan, H. Zhao, J. Qi, B. Ma, H. Fan, Boosting the electrochemical storage properties of Co_3O_4 nanowires by the Mn doping strategy with appropriate Mn doping concentrations, ACS Omega 9 (6) (2024) 6955–6964, https://doi.org/10.1021/acsomega.3c08650.

[42] A. Bhargava, C.Y. Chen, K. Dhaka, Y. Yao, A. Nelson, K.D. Finkelstein, C.J. Pollock, M.C. Toroker, R.D. Robinson, Mn cations control electronic transport in spinel $Co_xMn_{3-x}O_4$ nanoparticles, Chem. Mater. 31 (11) (2019) 4228–4233, https://doi.org/10.1021/acs.chemmater.9b01198.

[43] A.I. Hassan, S.I. Maki, Preparation and characterization of Cu:co_3O_4/Si heterojunction prepared by spray pyrolysis, Energy Proc. 119 (2017) 961–971, https://doi.org/10.1016/j.egypro.2017.07.129.

[44] C. Ravi Dhas, R. Venkatesh, R. Sivakumar, T. Dhandayuthapani, B. Subramanian, C. Sanjeeviraja, A. Moses Ezhil Raj, Electrochromic performance of chromium-doped Co_3O_4 nanocrystalline thin films prepared by nebulizer spray technique, J. Alloy. Compd. 784 (2019) 49–59, https://doi.org/10.1016/j.jallcom.2018.12.385.